Transcranial photoacoustic imaging of NMDA-evoked focal circuit dynamics in rat hippocampus

Jeeun Kang[1, 2], Shilpa D. Kadam[3], Joshua S. Elmore[1], Brennan J. Sullivan[4,*], Heather Valentine[1,*], Adarsha P. Malla[5], Maged M. Harraz[5], Arman Rahmim[1, 6], Jin U. Kang[2, 7], Leslie M. Loew[8], Michael Baumann[9], Anthony A. Grace[10], Albert Gjedde[1,11,12,13], Emad M. Boctor[1,2,7, 14,†], Dean F. Wong[1,5,15,16,†]

[1] Russell H. Morgan Department of Radiology and Radiological Science, Johns Hopkins University, Baltimore, MD, USA.

[2] Laboratory of Computational Sensing and Robotics, Whiting School of Engineering, Johns Hopkins University, Baltimore, MD, USA

[3] Neuroscience Laboratory, Hugo W. Moser Research Institute at Kennedy Krieger & Department of Neurology, Johns Hopkins Medical Institutions, Baltimore, MD, USA

[4] Neuroscience Laboratory, Hugo W. Moser Research Institute at Kennedy Krieger, Baltimore, MD, USA

[5] The Solomon H. Snyder Department of Neuroscience, Johns Hopkins University School of Medicine, Baltimore, MD, USA

[6] Departments of Radiology and Physics, University of British Columbia, Vancouver, BC, Canada

[7] Department of Electrical and Computer Engineering, Whiting School of Engineering, Johns Hopkins University, Baltimore, MD, USA

[8] Department of Cell Biology, University of Connecticut Health, Farmington, CT, USA

[9] National Institute on Drug Abuse, Intramural Research Program, NIH, Baltimore, MD

[10] Departments of Neuroscience, Psychiatry and Psychology, University of Pittsburgh, Pittsburgh, PA, USA

[11] Department of Neurology and Neurosurgery, McGill University, Montreal, Quebec, Canada

[12] Departments of Clinical Research and Nuclear Medicine, Odense University Hospital and University of Southern Denmark, Odense, Denmark

[13] Department of Neuroscience, University of Copenhagen, Copenhagen, Denmark

[14] Department of Computer Science, Whiting School of Engineering, Johns Hopkins University, Baltimore, MD, USA

[15] Department of Psychiatry and Behavioral Sciences, Johns Hopkins Medical Institutions, Baltimore, MD, USA

[16] Department of Neurology, Johns Hopkins Medical Institutions, Baltimore, MD, USA

*** Equal contribution**

† These authors share senior authorship and address all correspondence to: Dean F. Wong, E-mail: dfwong@jhmi.edu and to Emad M. Boctor, E-mail: eboctor1@jhmi.edu.

Keywords: Photoacoustic, neuroimaging, voltage-sensitive dye imaging, microdialysis, quantitative electroencephalogram, N-methyl-D-aspartate, glutamate, hippocampus

Abstract

Transcranial functional photoacoustic (fPA) voltage-sensitive dye (VSD) imaging promises to overcome current temporal and spatial limitations of current neuroimaging modalities. The technique previously distinguished global seizure activity from control neural activity in groups of rats. To validate the focal specificity of transcranial fPA neuroimaging *in vivo*, we now present proofs-of-concept that the results differentiate between low- and high-dose N-methyl-D-aspartate (NMDA) evoked neural activity in rat hippocampus. Concurrent quantitative EEG (qEEG) and microdialysis recorded real-time circuit dynamics and glutamate concentration change, respectively. We hypothesized that location-specific fPA VSD contrast would identify the neural dynamics in hippocampus with the correlation to NMDA evoked focal glutamate release and time-specific EEG signals. To test the hypothesis, we infused 0.3 to 3.0 mM NMDA at 2 μl/min over 60 min via an implanted microdialysis probe. The dialysate samples collected every 20 min during the infusion were analyzed for focal changes in extracellular glutamate release. Transcranial fPA VSD imaging provided NMDA-evoked VSD responses with positive correlation to extracellular glutamate concentration change at the contralateral side of the microdialysis probe. The graded response represents the all-or-none gating system of the dentate gyrus (DG) in hippocampus. Quantitative EEG (qEEG) successfully confirmed induction of focal seizure activity during NMDA infusion. We conclude that transcranial fPA VSD imaging distinguished graded DG gatekeeping functions, based on the VSD redistribution mechanism sensitive to electrophysiologic membrane potential. The results suggest the potential future use of this emerging technology in clinics and science as an innovative and significant functional neuroimaging modality.

Introduction

Whereas electrophysiological and invasive neurochemical techniques have been valuable in assessing activity within specific neural circuits in brain, there is a distinct need for a non-invasive means to image real-time regional functional activity in deep brain *in vivo*. The hippocampal circuit has rows of excitatory pyramidal neurons all aligned in close proximity with similar orientation. The dentate gyrus (DG) is classically considered as a gate keeper for the propagation of excitatory activity into the hippocampus as the excitatory neurons of the DG are less excitable than other types of hippocampal neurons. Therefore, low amplitude excitatory inputs do not generate action potentials in DG neurons and fail to open the DG gate [1]. In contrast to sub-threshold excitatory stimulus, strong repetitive excitatory inputs can break the DG gate and induce seizure activity [1]. This all-or-none gating function of the DG is consistent with the hippocampus being the lowest seizure threshold region of the mammalian brain.

Previous optical imaging approaches to local cortical circuits [2-4] applied invasive procedures to overcome superficial imaging depth, and further extension to deeper brain regions such as the hippocampus was prohibitive. The imaging of electrophysiological or neurochemical dynamics within the hippocampus primarily has been accomplished by optical imaging of freshly-sliced brain tissue [5] or magnetic resonance imaging spectroscopy (MRS) for non-invasive quantification of glutamate at high spatial resolution [6,7]. However, optical neuroimaging and MRS suffer from shallow imaging depth and from slow imaging speed, respectively. The application of two-photon microscopy to measure calcium ion dynamics in specific deep brain structures, including hippocampus, has poor temporal resolution [8]. Therefore, non-invasive, real-time neuroimaging modality having a high spatiotemporal resolution would be a significant advance, but such an approach would require neurochemical and electrophysiological characterization to validate the neural activity.

Photoacoustic (PA) imaging is a hybrid approach combining optics and acoustics where the signal corresponding to the neural activity is detected in the form of acoustic transcranial imaging with optical absorbance as an image contrast [9,10]. PA imaging is based on thermo-elastic perturbation of a target evoked by light absorbance from a pulsed laser illumination, which generates radio-frequency (RF) acoustic pressure waves detected by piezoelectric ultrasound transduction or optical interferometry. With this unique imaging mechanism, several attractive applications have been proposed for preclinical and clinical research with tomographic and microscopic imaging modes, including detection of endogenous contrast of cancer indicators, e.g., melanoma [11], breast microcalcifications [12-14], monitoring of cancer angiogenesis [15], oxygen metabolism [16], and quantification of lipid content [17,18], among others. Recently, we presented the functional PA (fPA) neuroimaging of near-infrared VSD redistribution mechanism differentiating the graded membrane potential in lipid vesicle model and chemo-convulsant seizure in rodent brain *in vivo* [19].

Here, we validated the transcranial fPA neuroimaging of hippocampal electrophysiology activated by stimulation of N-methyl-D-aspartate (NMDA) receptors in rat brain *in vivo* through intact skull and scalp. The tri-modal neural sensing approach utilized microdialysis, quantitative electroencephalography (qEEG), and transcranial fPA neuroimaging to simultaneously monitor electrophysiological changes associated with glutamatergic neurotransmission (Figure 1). To stimulate the hippocampus, we infused NMDA by reverse microdialysis that triggered localized changes of extracellular glutamate concentration. We quantified the change of extracellular glutamate concentration evoked by reverse microdialysis by direct microdialysis and high-performance liquid chromatography (HPLC). We combined fPA neuroimaging and qEEG with microdialysis to evaluate

103 the effects associated with graded DG gatekeeping at hippocampus, in the presence of glutamatergic
104 excitation. Concurrently, the electrophysiological signatures were captured with transcranial fPA
105 neuroimaging. Each of the three modalities thus provided information with different degrees of
106 specificity, including spatiotemporal specificity from fPA imaging, temporal specificity from qEEG,
107 and neurochemical specificity from microdialysis in the target neural circuit.

108

109 Results

110 **Transcranial fPA neuroimaging of rat hippocampus.** Transcranial fPA neuroimaging of
111 hippocampal circuit dynamics was performed during NMDA infusion at rat hippocampus (Figure 2).
112 The representative fPA sagittal planes obtained at 790 nm presented a sufficient sensitivity at the
113 depths of interest, i.e., 3.6 mm, at the contralateral position to the microdialysis probe (Figure 3a).
114 The sagittal PA imaging plane of hippocampus revealed the cross-sections of transverse sinus and
115 inferior cerebral vein in the superficial depth range (Figure 3b). From the temporal dimension, time-
116 averaged VSD responses were reconstructed pixel-by-pixel for pre-injection phase (-10 – 0 min)
117 followed by the results for time bins in 10 min interval: 0 – 10 min, 10 – 20 min, and 20 – 30 min.
118 Note that the total recording duration (40 min) was limited by internal memory of the fPA
119 neuroimaging system. Figure 3c shows the representative VSD responses in hippocampal cross-
120 sections collected during 0.3 mM and 3.0 mM NMDA infusion. As a result, the hippocampus with
121 0.3 mM NMDA infusion did not present such a significant change (n = 3), which implies a failure to
122 overcome the high activation threshold of DG gatekeeping with 0.3 mM NMDA infusion. Otherwise,
123 the substantial amount of circuit dynamics was detected at hippocampus with 3.0 mM NMDA
124 infusion (n = 6). In the 3.0 mM NMDA infusion group, the peak VSD responses were presented
125 during the first or second 10 min durations, and their peak intensities corresponds to the maximal
126 glutamate concentration change measured in the microdialysis, e.g., 734.48 % and 493.91 % (center
127 and right columns in Figure 3c). Further quantitative multi-modal correlation will be given in the
128 following subsections.

129 **NMDA-evoked glutamatergic neurotransmission.** Intrahippocampal infusion of NMDA diluted
130 into artificial cerebrospinal fluid at the required concentrations was performed through the
131 microdialysis probe. Concentrations of glutamate release in the dialysate were calculated from
132 values of three baseline samples collected at 20 min intervals before NMDA infusion. During
133 infusion into hippocampus (bregma -3.8 mm, lateral 3 mm, depth 3.6 mm; Figure 4a), samples
134 continued to be collected every 20 min for the remainder of the study. Glutamate release was
135 calculated as a % of basal values. Figure 4b shows the effect of NMDA infusion on
136 glutamate release in the hippocampus of anesthetized rats. The results demonstrate the dose-related
137 response of NMDA infusion at 0.3 (n = 3), 1.0 (n = 1), and 3.0 mM (n = 6) into the hippocampus,
138 where 0.3 mM NMDA caused a 17.93±19.05 % increase in glutamate levels that remained elevated
139 for the duration of the infusion; the 1.0-mM NMDA infusion appears to cause doubling of the
140 glutamate levels in the hippocampus compared to baseline (i.e., 112.42 %). This increase observed at
141 the 1.0-mM remained elevated through to the end of the NMDA infusion. However, at 3.0-mM, the
142 NMDA infusion raised the glutamate level up to 392.99±250.54 %, above baseline level, which
143 peaked during the second 20-min sampling period.

144 **EEG of electrophysiological activity in hippocampus.** The DG is a hippocampal region
145 specifically subjected to a barrage of excitatory inputs. However, the majority of excitatory activity
146 does not propagate through the DG and into the hippocampus as the DG performs a gating function [1].

147 Excessive activation of the DG disrupts its gating function and induces acute seizures in naïve
148 animals [1]. Hippocampal infusion of 3.0 mM NMDA induced a maximal VSD and significant rise in
149 extracellular glutamate concentration, suggesting a potential break in the DG gate that may lead to
150 acute seizure activity. We therefore utilized qEEG during the same hippocampal 3.0 mM NMDA
151 infusion protocol to identify if the maximal VSD response and extracellular glutamate concentrations
152 were associated with significant electrophysiological activity, a tri-modal approach that validates the
153 temporal and spatial resolution of fPA imaging during focal NMDA infusion.

154 In patients with focal epilepsy, gamma and theta activity from scalp EEG are an indicator of
155 the seizure onset zone and ictal onset [20,21]. Here, the temporal specificity of qEEG recorded circuit
156 responses in real-time, before and after focal NMDA infusion. The 3.0 mM NMDA infusion into the
157 hippocampal circuit induced focal seizure activity recorded on qEEG (Figure 4c black asterisk and
158 S1). When NMDA was delivered to the hippocampal circuit by the microdialysis probe (Figure 4a)
159 [22], a significant change in qEEG spectral power was presented, especially in the gamma range (Figure
160 4c). In the theta range, spectral power increased during the seizure (Figure 4d) further supporting the
161 identification of the focal seizure activity. The seizure trace on EEG demonstrated both a gamma and
162 theta component (Figure 4f). Importantly, the ictal event occurred during the same temporal window
163 as the maximum VSD response and the greatest increase in extracellular glutamate concentration.
164 The dose-related VSD and extracellular glutamate concentration response with qEEG suggest that the
165 3.0-mM NMDA infusion resulted in a break in the DG gate associated with focal seizure activity.

166 However, qEEG lacks spatial resolution, and recordings from deep brain structures cannot be
167 isolated without implantation of invasive depth electrodes. Therefore, in order to maintain the tri-
168 modal experimental paradigm we opted not to place depth electrodes. We made the stimulation
169 focal, according to the previous proof-of-concept results by fPA detection onset of generalized
170 seizures through an intact skull and scalp [19].

171 **Quantitative multi-modal correlation.** The fPA VSD responses at the contralateral side to the
172 microdialysis probe (blue dots in Figure 3c) were measured and plotted as a function of the
173 corresponding changes in extracellular glutamate concentration (Figure 5). Note that the regions-of-
174 interest ROIs to quantify the VSD responses were in 1 x 1 mm^2 size in the sagittal cross-section of rat
175 hippocampus. The reference phase for VSD response quantification was obtained from the baseline
176 phase: 5 – 10 min. In fPA imaging, 3.0 mM NMDA infusion at hippocampus yielded significant
177 elevation of VSD response: 0.08±0.35, 2.24±1.06, and 1.17±1.56 for baseline (-10 – 0 min), NMDA1
178 (0 – 20 min), and NMDA2 (20 – 30 min) phases, respectively (Figure S2a). The increase of
179 glutamate concentration change was correspondingly presented from -4.67±4.48 %, 369.75±254.91
180 %, to 392.99±250.54 %. In addition, when re-analyzing the data for -50 – 100 %, 100 – 500 %, and
181 500 – 1,000 % bins of fractional glutamate concentration change, high positive correlation was
182 obtained with VSD responses: 0.38±0.55 (n_{sample} = 9), 0.97±1.40 (n_{sample} = 5), and 3.17±0.32 (n_{sample}
183 = 4) for 11.04±29.60 %, 279.85±141.64 %, to 666.49±73.63 % of glutamate concentration changes
184 (red lines in Figure 5). The goodness of fit (R^2) among the mean values was 0.95 with slope and y-
185 intercept at 0.12 and 0.00, respectively. The qEEG found the increased bursts of gamma power
186 during 3.0 mM NMDA infusion, reaching up to ~261 % increase with a focal seizure (Figure 4c and
187 S1). Otherwise, focal 0.3 mM NMDA infusion at hippocampus did not presented any circuit
188 activity increase statistically significant. The VSD responses were -0.11±0.02, -0.15±1.71, and -
189 0.07±0.64 in baseline, NMDA1, and NMDA2 phases, respectively, which are correlated to the low
190 glutamate concentration changes in hippocampus: -1.65±6.90 %, 3.90±10.41 %, and 17.93±19.05 %
191 (Figure S2b). Also, the VSD responses presented strong positive correlation when re-analyzed in -10
192 – 0 %, 0 – 10 %, and 10 – 50 % bins of fractional glutamate concentration changes: -1.00±1.00,

193 0.10±0.35, and 0.58±0.48 (n_{sample} = 3 for each) with -6.84±3.38 %, 4.43±4.05 %, and 22.59±11.64 %
194 of fractional glutamate concentration changes, respectively (blue lines in Figure 5). The R^2 was 0.88
195 with slope and y-intercept at 0.05 and -0.46, respectively.

196 **Brain histology.** Brain tissue was extracted after all *in vivo* experimental protocols. The brain was
197 frozen-sectioned into 300-µm thickness slices and evaluated to confirm probe placement using the
198 hemorrhage caused by the microdialysis probe insertion for the NMDA infusion and collections as a
199 marker. Figure 6a shows the bright-field images of the coronal plane of the hippocampus at -3.8 mm
200 from bregma, respectively. White arrows indicate the hemorrhage caused by the microdialysis probe
201 positioned at the following coordinates in hippocampus: bregma -3.8 mm, lateral 3 mm, and depth
202 3.6 mm. The VSD staining of brain tissue was confirmed with near-infrared fluorescence
203 microscopy. Uniform VSD fluorescence was found in the VSD perfusion animal, while negative
204 control (VSD-) presented negligible fluorescence emission (Figure 6b), which again confirms the
205 results in our previous publication [23].

206

207 Discussion

208 The application of fPA neuroimaging was expanded to neuroscience [24-26] as label-free transcranial
209 fPA imaging of neurovascular coupling proposed as a means to quantify hemodynamic changes [27,28].
210 However, this approach does not yield quantitative neural activities that directly correspond to
211 electrical activity. Hemoglobin provides an effective contrast signal in fPA neuroimaging, but the
212 neurovascular coupling in brain is comparatively slow compared to electrophysiological neural
213 activities. Instead, there has been extensive investigations into more effective exogenous contrast
214 agents [29-33]. This approach has enabled several neuroimaging approaches with functional voltage
215 sensors. Deán-Ben et al. showed real-time PA tomography of a genetically encoded calcium
216 indicator, GCaMP5G, using zebrafish *in vivo* [34]. Sheryl Roberts, et al. also proposed a new
217 metallochromic calcium sensor for PA imaging (CaSPA) which has a high extinction coefficient, a
218 low quantum yield, and high photo-bleaching resistance for brain and heart imaging [35]. Ruo et al.
219 reported PA imaging of neural activity evoked by electrical stimulation and 4-aminopyridine-induced
220 epileptic seizures using hydrophobic anions such as dipicrylamine (DPA) in mouse brain [36].
221 However, these voltage sensors requires PA imaging at the visible spectral range (488 nm and 530
222 nm for GCaMP5G; 550 nm for CaSPA; 500 nm and 570 nm for DPA), which are suboptimal when
223 imaging deep brain such as hippocampus positioned at 5 mm – 8 mm depth including intact scalp and
224 cortex in rat [22,37].

225 Recently, we proposed transcranial fPA recordings of brain activity *in vivo* with a near-
226 infrared VSD, delivered through the blood-brain barrier (BBB) via pharmacological modulation, as a
227 promising tool to transcend optical neuroimaging limitations, particularly as it relates to sensing
228 depth [19,23,38]. The studies demonstrated that transcranial fPA neuroimaging distinguishes *in vivo*
229 seizure activity in stimulated rat brains from that of control groups in real time. However, the results
230 were limited by the use of a global chemo-convulsant, causing perturbation across the entire brain
231 caused by the intraperitoneal administration of penetylenetetrazole (PTZ). In this paper, we presented
232 follow-on advances in fPA VSD neuroimaging by focal neural stimulation of heterogeneous neural
233 circuits, with concomitant validations from qEEG and glutamate quantification using microdialysis,
234 respectively. The set of experiments described here yield key findings as follows: (1) The
235 microdialysis-dependent low- and high-dose NMDA infusion into the central nervous system (CNS)
236 lead to a wide range of focal extracellular glutamate concentration increase in hippocampus up to

237 ~800 %. (2) The neurochemical response (microdialysis) was well-correlated to the phenotypes in the
238 electrophysiological sensing (qEEG). The NMDA activation in the hippocampus triggers an all-or-
239 none type of circuit dynamics that lead to the initiation of a focal seizure in the hippocampal circuit.
240 (3) Transcranial fPA neuroimaging data successfully identified hot spots of focal NMDA receptor
241 activation, as presented in the qEEG recordings. The hippocampal circuitry provided the proportional
242 excitation of glutamatergic neurotransmission with concomitant NMDA infusion. The DG of the
243 hippocampus is positioned as a gatekeeper to regulate the vast excitatory cortical inputs from
244 propagating into the hippocampus [1]. Characteristically, the DG displays a high activation threshold; a
245 trait that is mediated by its profuse innervation by inhibitory GABAergic neurons and relatively
246 hyperpolarized resting membrane potential of its pyramidal neurons [39]. In epilepsy the DG fails to
247 gate the propagation of excitatory inputs into the hippocampus, resulting in overexcitation and
248 seizures. In naïve animals, *in vivo* optogenetic activation of the DG disrupts its gating function and
249 induces seizures that increase in severity depending on the duration of the stimulus [1]. In this study,
250 the disruption of DG gating by strong stimuli has been clearly demonstrated by utilizing the fPA
251 VSD neuroimaging techniques during focal NMDA infusion.

252 Further investigations are required to advance our current perspectives available with tri-
253 modal sensing, including fPA, qEEG, and microdialysis. Glutamate produces fast-rising brief
254 depolarizations in pyramidal neurons. Therefore, the use of fPA neuroimaging will enable us to more
255 precisely assess glutamate and GABA dynamics in order to formulate a more complete profile of
256 circuit activation. Once homeostasis is disrupted, neuronal activity is sensitive to changes both of
257 excitatory and inhibitory mechanisms. Faster neurochemical recording is another approach that may
258 prove useful in assessing the impact of these measures. Although microdialysis successfully
259 provided quantitative, focal neurochemical concentrations, the sampling rate of 1 sample per 20 min
260 was slow. Techniques offering faster temporal resolution may allow more meaningful comparison of
261 the neurochemical changes yielded by microdialysis and the electrophysiological events monitored
262 by qEEG and fPA neuroimaging [40]. One such technique, using custom built hardware and the
263 Amplex Red method, achieved fluorescence-based quantification of glutamate from samples taken
264 every 5 seconds, though reliability appeared to be limited when higher glutamate concentrations were
265 measured [41]. Implantable glutamate biosensors allow sub-second readouts of neurochemical
266 concentrations. However, current limitations include sensitivity, selectivity, and high cost; recent
267 developments in materials, effective modeling, and sensor design may soon alleviate some of these
268 limitations [42,43].

269 From the results, transcranial fPA neuroimaging was able to differentiate the circuit activity
270 defined with qEEG and microdialysis. However, future developments should serve to further advance
271 the efficacy of the fPA neuroimaging in neuroscience. (1) We expect that improved signal processing
272 for extracting neural activity from the ubiquitous blood context will enable better characterization of
273 brain function. The present *in vivo* experiments confirmed the possibility of background suppression,
274 as also presented in our previous study [19]. Enhanced signal processing and/or use of multi-spectral
275 wavelengths may allow significantly improved spectral differentiation of electrophysiological
276 activities in the brain at higher temporal resolution, leading to development of novel quantitative
277 metrics for real-time brain activity measures. Having isotropic resolution with 2-D PA probes would
278 be also an interesting direction to pursue as a follow up to the present work. The use of 2-D PA probe
279 would not only allow real-time volumetric information, but also enable the suppression of off-axis
280 interference. Even though we presented that neural activity can be successfully discerned with our
281 current 1-D PA probe, its sensitivity might be affected by off-axis interferences especially from the
282 elevation direction because of the limited acoustic lens focusing at a fixed depth. The neuroimaging
283 using 2-D PA probe would reject those interferences by the advanced electrical beamforming

capability in axial, lateral, and elevation directions. Having an improved PA imaging system would provide significant breakthrough in terms of spatiotemporal resolution in fPA neuroimaging. Even though our current laser system yields both 4 fps (frame-per-second) of temporal resolution and PA signal sensitivity at rat hippocampus, further optimization of temporal resolution would provide finer spatiotemporal specificity. On the other hand, we consider employing larger animal model for this fPA VSD neuroimaging research. Pig models have been an ideal subject to pave the way to human translation of neuroengineering technologies, thanks to their analogous brain structure and physiology and scalp and skull thicknesses to those in humans, with alleviated ethical issues [44]. We already validated the transcranial fPA neuroimaging in the pig model, and will continue to pursue this research direction [45].

In all, the transcranial fPA neuroimaging at hippocampus in *in vivo* rat brain was successfully correlated with electrophysiologic and neurochemical measurements using qEEG and microdialysis: focal NMDA infusion triggers glutamate release that excites the neural circuit, and at threshold doses it causes runaway excitation in the hippocampus by overcoming DG gating. This is reflected in the lower seizure threshold of the hippocampus. Therefore, the transcranial fPA neuroimaging is a promising technology for the visualization of focal neural events in real time.

Material and Methods

Animal preparation. For the proposed *in vivo* experiments, 8-9-week-old male Sprague Dawley rats (Charles Rivers Laboratory, Inc., MA, United States) weighing 275-390g were used. The use of animals for the proposed experimental protocol was approved by the Institutional Animal Care and Use Committee of Johns Hopkins Medical Institute (RA16M225). Rats were housed in groups of 3 per cage with free access to food and water and maintained on a 12hr light / 12hr dark cycle.

On the day of the study the rats were weighed and anesthetized with urethane (1.2mg/kg,). Urethane was given incrementally with alternating intra-peritoneal (ip) and subcutaneous (sc) dosing. Three (3) ml of isotonic saline was given sc on each side of the body to keep the animal hydrated during the experimental procedure. Body temperature was maintained until animal was fully anesthetized and ready for surgery. For fPA and qEEG studies, an iv catheter was inserted into a tail vein prior to surgery for dye administration during the studies. Once a stable plane of anesthesia was established, hair was shaved from the scalp of each rat to have acoustic coupling for transcranial fPA recording. The rat was placed into a stereotaxic device (Stoeling Co. Wood Dale, IL). This fixation procedure was required to prevent any unpredictable movement during fPA or EEG recording of neural activities. A CMA12 microdialysis probe (Harvard Apparatus, Holliston, MA, USA) was implanted into the CA_3 region of the right hippocampus (stereotaxic coordinates: 3 mm lateral and 3.8 mm posterior to bregma, and 3.6 mm below the surface of the dura, Figure 3a) [22]. The probe active exchange surface was 2 × 0.5 mm. The probe was secured to the skull using dental acrylic cement. The fPA and qEEG probes were placed on the contralateral side of the microdialysis probe.

Fluorescence quenching-based near-infrared voltage-sensitive dye. In the present *in vivo* study, we used the fluorescence quenching-based near-infrared cyanine VSD, IR780 perchlorate (576409, Sigma-Aldrich Co. LLC, MO, United States) as used in our previous *in vivo* study differentiating a chemo-convulsant seizure activity [19], and it has the analogous chemical structure of PAVSD800-2, our new VSD validated in our previous *in vitro* study [38]. This VSD yields fluorescence quenching and de-quenching depending on membrane polarization and subsequent change in the local VSD

327 molecule density, leading to a reciprocal change of PA contrast with non-radiative relaxation of
328 absorbed energy.

329 **Functional fPA neuroimaging.** We used real-time PA data acquisition to record
330 electrophysiological neural activities *in vivo* as in our previous study [19]: an ultrasound research
331 system consisted of an ultrasound linear array transducer connected to a real-time data acquisition
332 system (SonixDAQ, Ultrasonix Medical Corp., Canada). To induce the PA signals, pulsed laser light
333 generated by a second-harmonic (532 nm) Nd:YAG laser pumping an optical parametric oscillator
334 (OPO) system (Phocus Inline, Opotek Inc., USA) provided 690-900 nm of tunable wavelength range
335 and 20 Hz of the maximum pulse repetition frequency. A bifurcated fiber optic bundle, each 40 mm
336 long and 0.88 mm wide, was used for laser pulse delivery. The PA probe was situated between the
337 outlets of the bifurcated fiber optic bundles using a customized, 3-D printed shell for evenly
338 distributing laser energy density in the imaging field-of-view. The alignment of outlets was focused
339 specifically at 20 mm depth. The PA probe was positioned in the contralateral sagittal plane of
340 microdialysis probe (3 mm) to cover the hippocampal cross-section. The distance between the PA
341 probe and the rat skin surface was 20 mm filled with acoustic gel, and the resultant energy density
342 was at ~3.5 mJ/cm^2 , which is far below the maximum permissible exposure (MPE) of skin to laser
343 radiation by the ANSI safety standards [46]. A wavelength of 790 nm was used, at which sufficient
344 absorbance can be obtained by the near-infrared VSD, i.e., IR780 perchlorate. Also, excitation at that
345 wavelength prevented the undesired time-variant change of blood oxygen saturation, since the
346 wavelength corresponds to the isosbestic point of Hb and HbO_2 absorption spectra. Detailed
347 information of neural activity reconstruction using normalized time-frequency analysis can be found
348 in our previous publication [19].

349 ***In vivo* microdialysis**. *In vivo* microdialysis sampling was carried out as previously described [47,48].
350 For infusion experiments, NMDA (Sigma-Aldrich Chemicals, St. Louis, Mo) was weighed,
351 solubilized, and diluted to the desired concentration in artificial cerebrospinal fluid (NaCl, 147
352 mmol/L; KCl, 2.7 mmol/L; $CaCl_2$, 1.2 mmol/L; $MgCl_2$, 0.85 mmol/L) (Harvard Apparatus, Holliston,
353 MA, USA) on the study day. Once the probe was inserted and secured, it was perfused with artificial
354 cerebrospinal fluid pumped at a flow rate of 2 µl/min. Samples were collected at 20 min intervals,
355 and immediately transferred to a -80°C freezer until assayed. To allow sufficient time for the
356 glutamate levels to equilibrate, three baseline samples were collected an hour following initiation of
357 infusion. Following these samples, NMDA was infused into the brain directly through the dialysis
358 probe with the same pump parameters as used for the baseline samples. Dialysate samples were
359 assayed for glutamate by a two-step process using HPLC-ECD on an Eicom HTEC-500 system
360 (EICOM, San Diego, CA, USA). After passing the samples through a separation column, they were
361 processed via a column containing immobilized L-glutamate oxidase enzyme, resulting in the release
362 of hydrogen peroxide. The hydrogen peroxide concentration was then determined using a platinum
363 working electrode. Chromatographic data were acquired online and exported to an Envision software
364 system (EICOM, San Diego, CA, USA) for peak amplification, integration, and analysis.

365 **Quantitative EEG.** All EEG recordings utilized a three-electrode paradigm: 1 recording, 1 reference
366 (aligned to the site of activation) and 1 ground over the rostrum. The electrodes (IVES EEG; Model #
367 SWE-L25 – IVES EEG solutions, MA, USA) were fixed with minimal cyanoacrylate adhesive
368 (KrazyGlue), similar to previous protocols [49]. Data acquisition was performed using Sirenia software
369 (Pinnacle Technologies Inc., Kansas, USA) with synchronous video capture. Data acquisition had a
370 14-bit resolution, 400 Hz sampling rate, and a band pass filter between 0.5 Hz and 50 Hz. The
371 acquisition files were stored in an .EDF format and scored manually, using real-time annotations

372 from the experiments. EEG power for 2-second epochs was done using an automated fast Fourier
373 transformation module in Sirenia software [50].

374 ***In vivo* experimental protocol.** The *in vivo* protocols were designed for simultaneous multi-modal
375 sensing of the neural activity at hippocampus: microdialysis-qEEG and microdialysis-fPA
376 neuroimaging. Figure 2 shows a detailed schematic protocol for each group representing the response
377 to the administration of NMDA, Lexiscan and VSD (i.e., IR780 perchlorate). fPA and qEEG data
378 acquisition were performed for 40 min to correlate with three microdialysis samples collected at 20-
379 min intervals. Graded NMDA infusion concentrations were applied to identify the dose-dependent
380 glutamatergic excitation of hippocampal circuit: 0.3 mM (n = 3) and 3.0 mM (n = 6). VSD and
381 Lexiscan followed the data acquisition sequence with 3-min delay, thereby 5 min of baseline phase
382 was guaranteed for the VSD response reconstruction in fPA neuroimaging before starting NMDA
383 infusion. The dosing protocol for Lexiscan and VSD administration was as follows: through an iv tail
384 vein catheter, 150 µl of Lexiscan (0.4mg/5ml) was injected, followed by 200 µl of VSD at 2 mg/ml
385 concentration, flushed immediately with 150 µl of 0.9% isotonic saline. The EEG signal was
386 recorded an identical preparation procedure as the fPA neuroimaging, including animal preparation
387 and administration of IR780, Lexiscan and experimental duration time for all recordings.

388 **Brain histology.** Rats used for the above protocol were sacrificed, and whole brains immediately
389 harvested and placed in 10 % formalin. All brains were allowed to fix in fresh 10 % formalin for at
390 least 48 hours with gentle agitation on a conical rotator. Subsequently, the brains were processed
391 through a series of sucrose gradients (15 %, 20 %, 30 % for 12-24 hours each) for cryoprotection.
392 Brains were sectioned frozen at 300 µm thickness. Tissue sections were mounted on slides in
393 ProLong Diamond Anti-face mountant. Slides with sections were imaged using an Olympus OM-D
394 E-M5 Mark II for bright field image and using LI-COR Odyssey for fluorescence visualization.

395

Author Contributions

DFW, AAG and MB originally conceived of the NMDA administration and of microdialysis with PA idea and helped to design the overall research plan with initial funding for the *in vivo* experiments. DFW critically revised the focus of the results and final version and interpretation. EMB, LML, and SDK helped to design the overall research plan, helped plan specific experiments and all contributed to the review and writing of the manuscript. Jeeun K, SDK, JSE, BJS, HV planned and carried out *in vivo* experiments, analyzed the research outcomes, and wrote key elements of the first draft of the manuscript. Jeeun K analyzed and interpreted the PA measurements and completed the first manuscript, HV and JE the NMDA dosing and microdialysis, and SDK and BS the EEG experiments. MB provided resources and personnel and vital collaboration for the microdialysis part of the experiment. HV and LML devised the VSD vehicle preparation. APM performed histopathological analysis. MMH planned and supervised confirmation of VSD penetration into brain tissue also contributed to the final version of the manuscript. AAG critically revised experimental design, draft, and final versions of manuscript, and interpretation of results. Jin K developed, funded, and participated in the current PA system design. AR participated in early planning and critically read and edited the manuscript. He has contributed both technically and materially to support this research. EMB led the development, system specification, design specification, and funding of the current PA imaging system. Secured the funding of the needed imaging experiments throughout the lifetime of the project, including taking responsibility of 2 full-time research members specifically for this work, Jeeun K and APM. Further, he has contributed intellectually by mentoring these members and providing input on manuscripts, and participating on PI meetings.

Funding

This work was supported by the NIH BRAIN Initiative under Grant No. R24 MH106083-03 (DFW, AR, AAG, EMB, HV, JE) and the NIH National Institute of Biomedical Imaging and Bioengineering under Grant No. R01EB01963 (LML); NIH National Institute of Child Health and Human Development (NICHD) for R01HD090884 (SDK); NIH National Institute of Heart, Lung and Blood (NHLBI) under grant number R01HL139543 (Jeeun K, APM, EMB); National Cancer Institute (NCI) under grant number R21CA202199 and its equipment supplement (EMB). Funding of the PA equipment was provided via resources of Jin K and EMB NSF Career award #1653322. Jeeun K was partially supported by the Basic Science Research Program through the National Research Foundation of Korea (NRF) funded by the Ministry of Education #2018R1A6A3A03011551.

Conflict of Interest Statement

The subject matter described in this article is included in patent applications filed by the University of Connecticut and Johns Hopkins University. LML is a founder and owner of Potentiometric Probes LLC, which sells voltage sensitive dyes.

The remaining authors declare that the research was conducted in the absence of any commercial or financial relationships that could be construed as a potential conflict of interest.

435 **Figures**

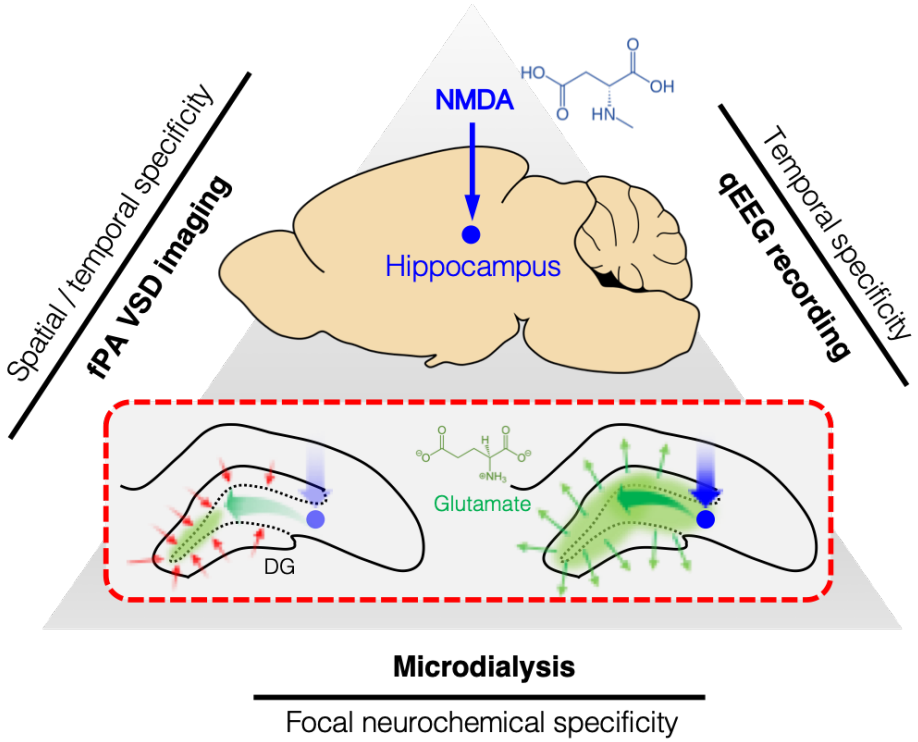

436

437 **Figure 1 Tri-modal sensing of rat hippocampus.** Red dotted rectangular describes dentate gyrus (DG)
438 gating breakdown at hippocampus to a focal NMDA infusion. NMDA, N-methyl-d-aspartate; VSD, voltage-
439 sensitive dye.

440

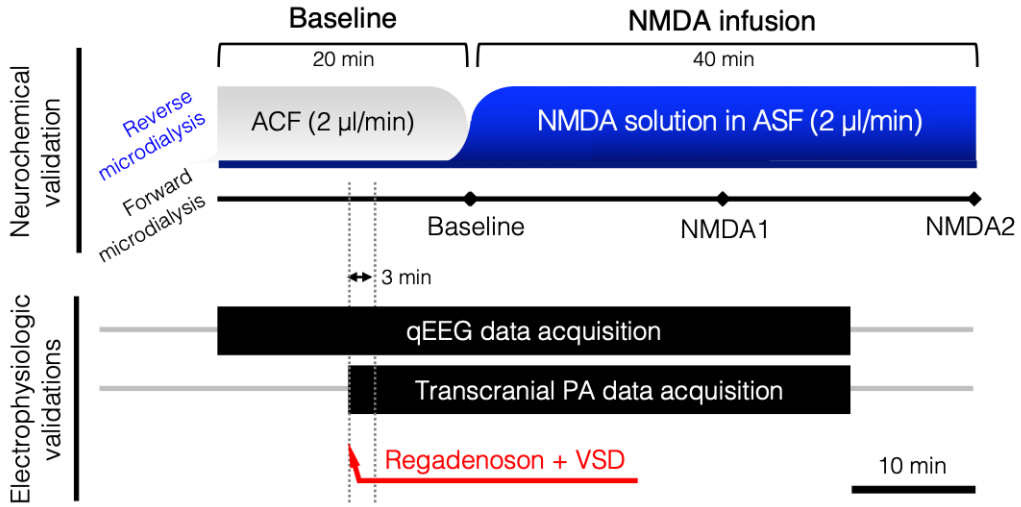

441

442 **Figure 2 *In vivo* experimental protocol.** Tri-modal monitoring of rat hippocampus using reverse/forward
443 microdialysis, transcranial PA imaging, and qEEG. ACF, artificial cerebrospinal fluid.

444

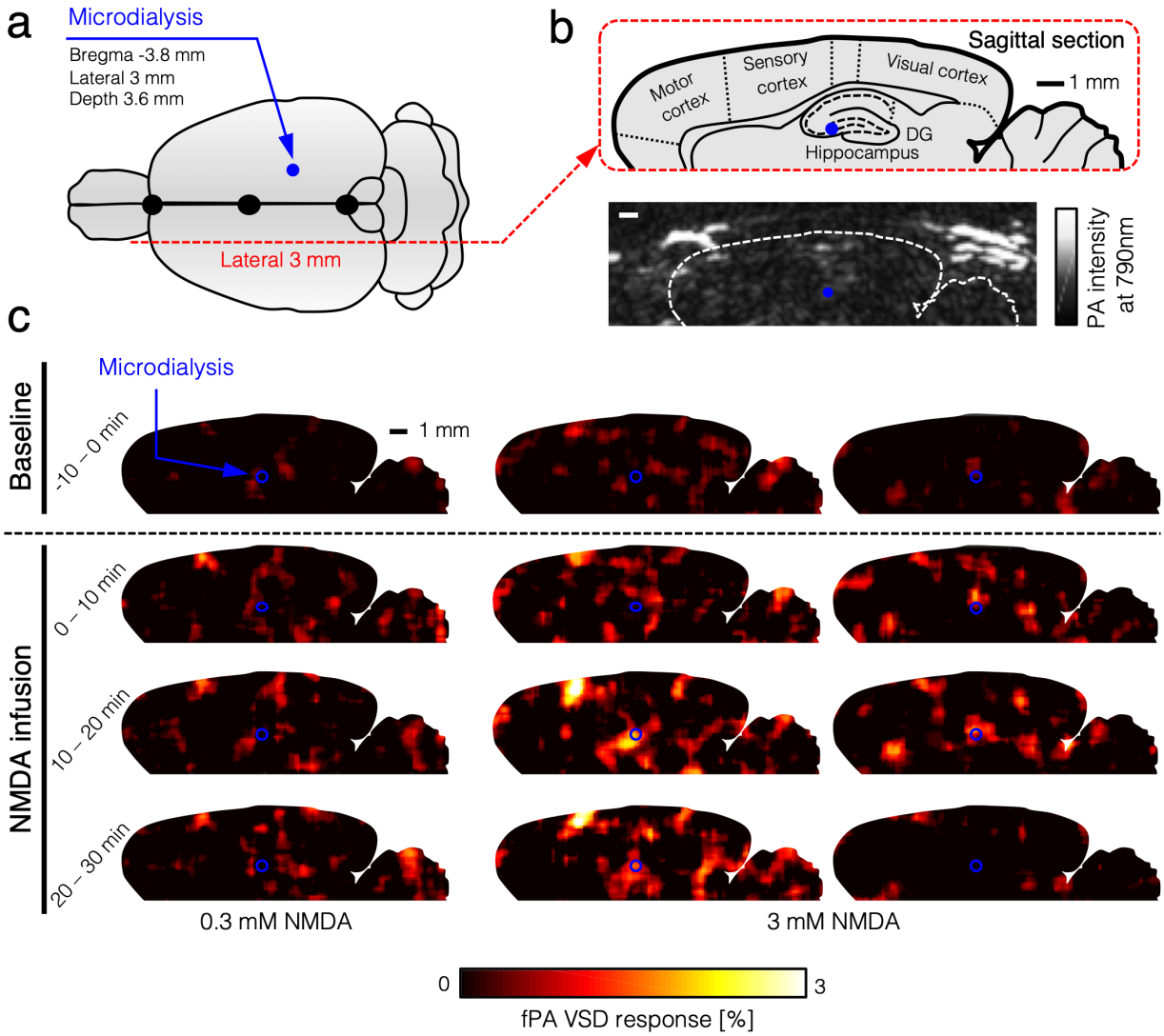

Figure 3. Transcranial PA neuroimaging of the hippocampal circuit dynamics following focal NMDA infusion. (**a**) Illustration of stereotaxic coordinates for the microdialysis probe and sagittal cross-sections for real-time PA recording. (**b**) The sagittal PA imaging plane was selected in the contralateral side of the microdialysis probe infusing NMDA into the brain (3 mm lateral). (**c**) Time-averaged VSD response maps during -10 – 0 min (baseline phase); 0 – 10 min, 10 – 20 min, and 20-30 min (NMDA infusion phases). Note that the blue points indicate microdialysis probe in contra-lateral positions. Maximal glutamate concentration increases for representative fPA images were 34.23 % (left), 734.48 % (center) and 493.91 % (right).

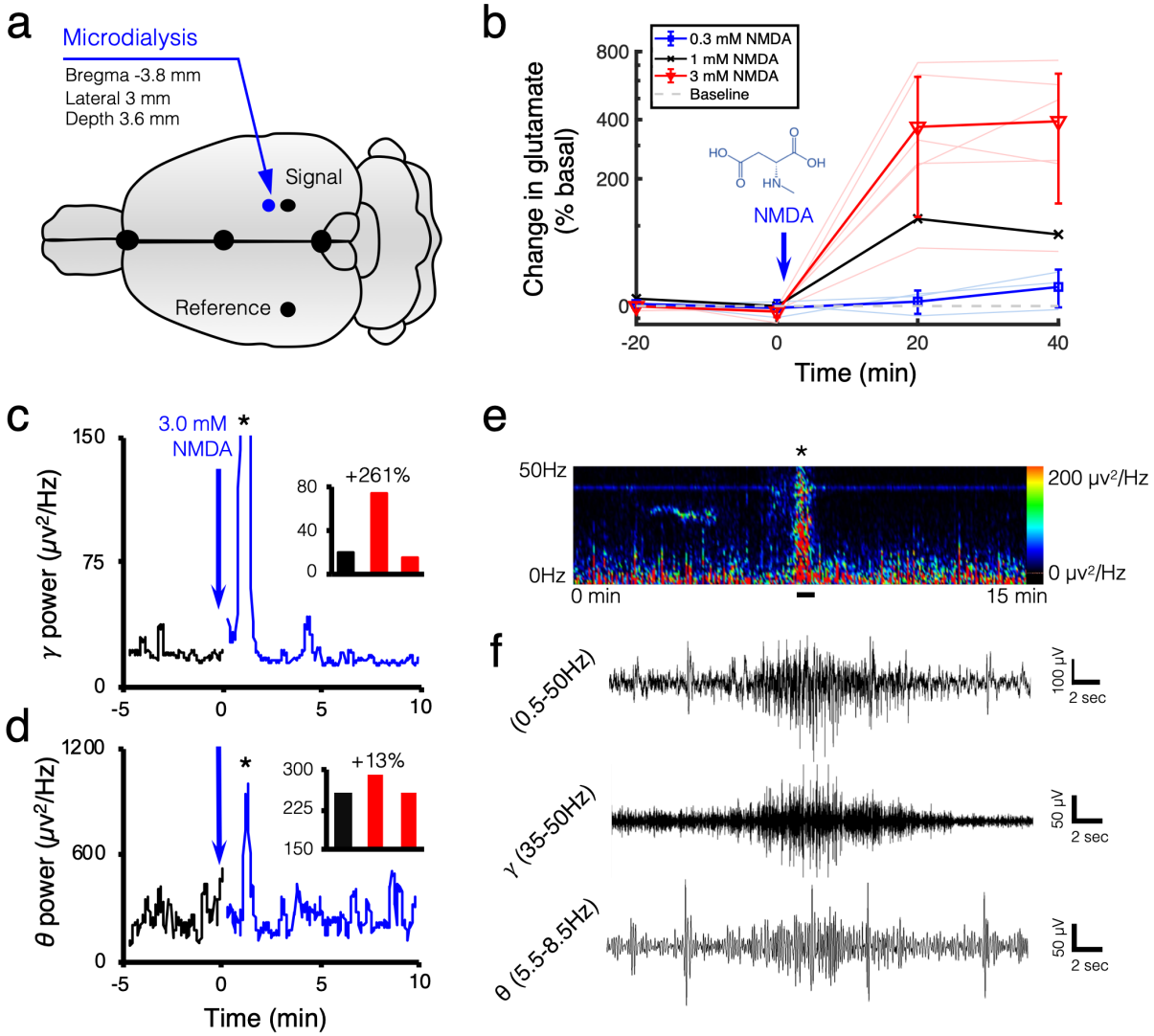

Figure 4. Extracellular glutamate concentration and concomitant electrophysiology during NMDA-evoked activity in the hippocampus. (**a**) Illustrates stereotaxic coordinates for the microdialysis probe and recording leads. Ground electrode was implanted over the rostrum. (**b**) 0.3 (n = 3), 1.0 (n = 1), and 3.0 mM (n = 6) NMDA infusion into the hippocampus caused maximal glutamate increases of 17.93±19.05%, 112.42%, and 392.99±250.54% respectively as compared to % baseline. Gray dotted line indicates the baseline. (**c**) Gamma (35-50Hz) power shows a 5-min baseline recording (black trace), followed by two consecutive 5 min traces (blue trace) following focal NMDA infusion in the hippocampus. EEG demonstrated a 261% increase in gamma power, as compared to % baseline, and an onset of epileptiform discharges after focal NMDA infusion (see inset bar graph; asterisk denotes epileptiform activity). (**d**) Respective theta power after NMDA infusion represents the theta component of the focal seizure. (**e**) 15-min spectral power heat map demonstrates the spectral power changes associated with NMDA infusion and subsequent epileptiform activity (denoted by black asterisk in e). (**f**) The representative raw EEG trace during the occurrence of the epileptiform event (solid black line in e) for full (05.-50Hz), gamma (0.5-50Hz), and theta (5.5-8.5Hz) power; respectively. For the expanded time scale of the focal hippocampal seizure see Supplemental 1.

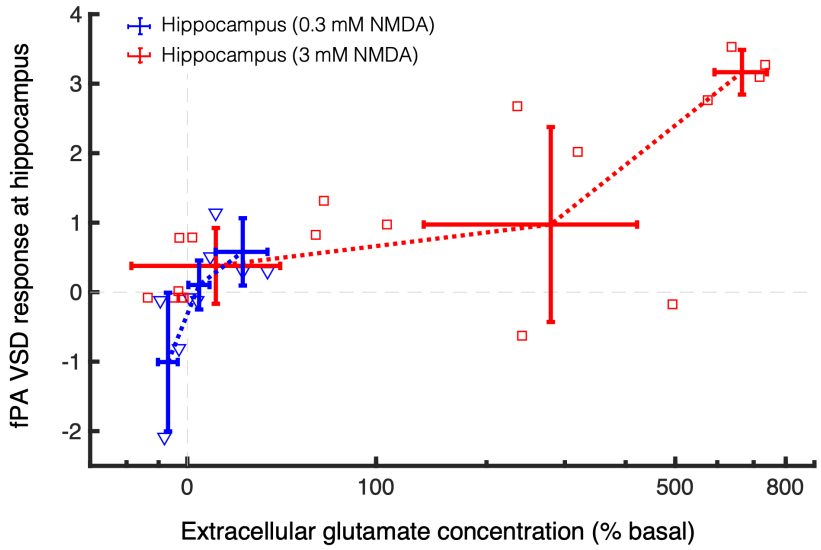

Figure 5. fPA VSD response at hippocampus as a function of extracellular glutamate concentration change. Grey dotted lines indicate the basal level in fPA VSD response and extracellular glutamate concentration.

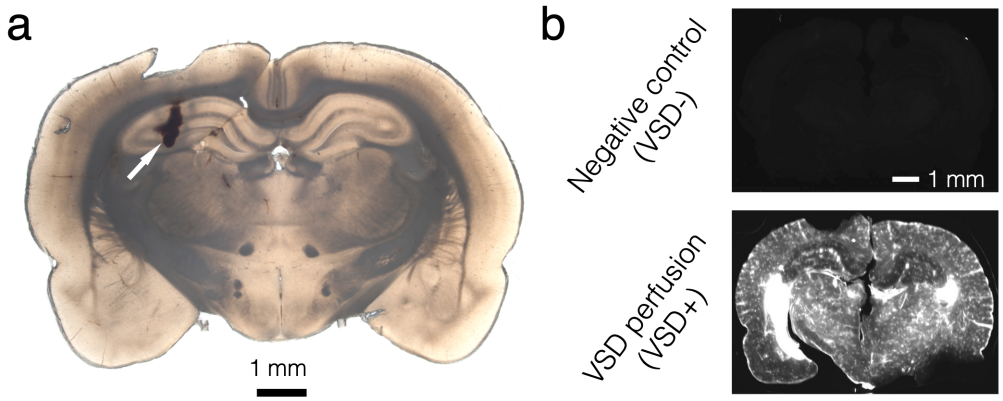

Figure 6. Histopathological confirmation (**a**) Microdialysis probe at hippocampus. White arrow indicates the wound caused by microdialysis probe installation. (**b**) Frozen-sectioning histopathological confirmation of systematic VSD delivery throughout brain tissue region.

Supplementary Material

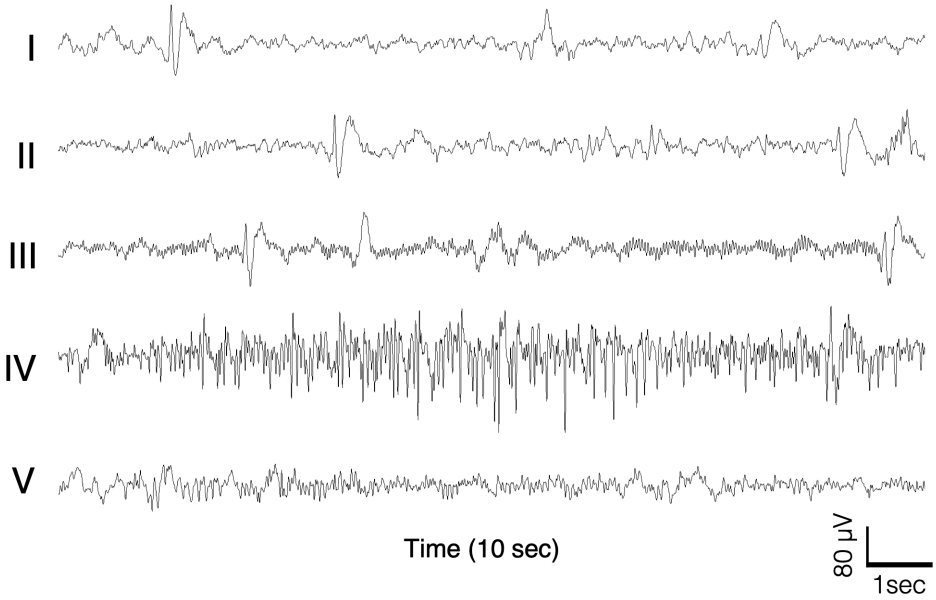

Figure S1. Expanded time scale of EEG recording during NMDA infusion into the hippocampus. (**a**) 10 sec expanded time scale of raw EEG traces during hippocampal NMDA infusion. (I) Baseline (II) immediately after onset of NMDA infusion (III) immediately before ictal event (IV) during focal seizure event (V) and sustained short duration high frequency hippocampal discharges after the focal seizure event.

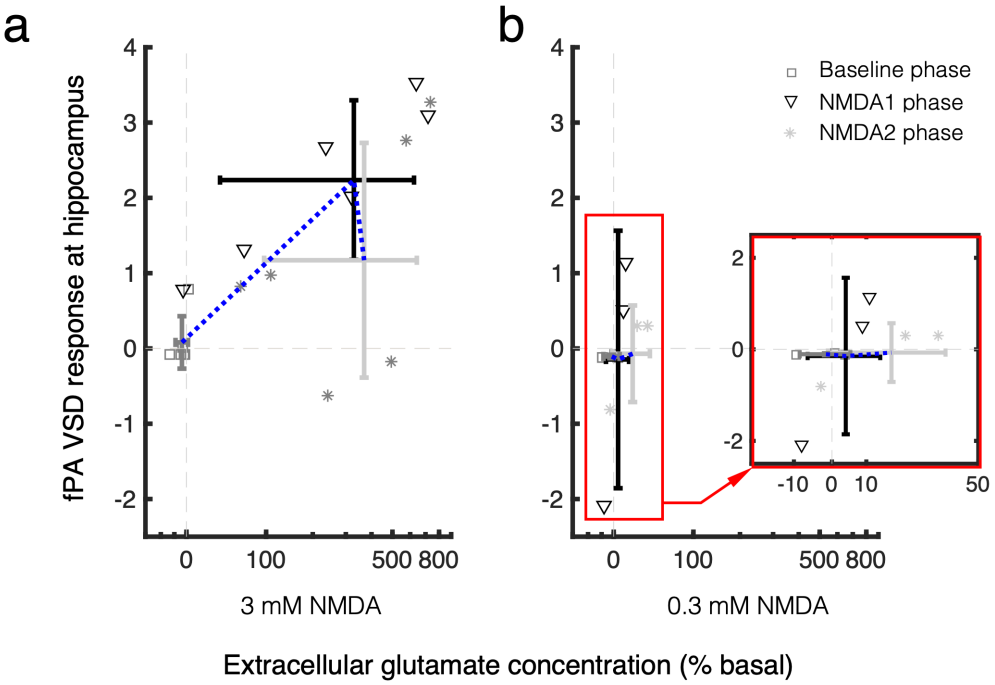

488 **Figure S2. fPA VSD responses in baseline, NMDA1, and NMDA2 phases as a function of extracellular**
489 **glutamate concentration change at hippocampus.** (**a**) 3.0 mM NMDA infusion. (**b**) 0.3 mM NMDA
490 infusion. 0.3 mM NMDA data in red rectangular is magnified and presented together (see inset graph). Grey
491 dotted lines indicate the basal level in fPA VSD response and extracellular glutamate concentration.

492 **References**

493 1 Magnuson EK, Armstrong C, Bui A, Lew S, Oijala M, Soltesz I. In vivo evaluation of the
494 dentate gate theory in epilepsy. *The Journal of Physiology* 2015; **593**: 2379–2388.

495 2 Derdikman D, Hildesheim R, Ahissar E, Arieli A, Grinvald A. Imaging spatiotemporal
496 dynamics of surround inhibition in the barrels somatosensory cortex. *J Neurosci* 2003; **23**:
497 3100–3105.

498 3 Petersen CCH, Grinvald A, Sakmann B. Spatiotemporal Dynamics of Sensory Responses in
499 Layer 2/3 of Rat Barrel Cortex Measured In Vivo by Voltage-Sensitive Dye Imaging Combined
500 with Whole-Cell Voltage Recordings and Neuron Reconstructions. *Journal of Neuroscience*
501 2003; **23**: 1298–1309.

502 4 Petersen CC, Sakmann B. Functionally independent columns of rat somatosensory barrel cortex
503 revealed with voltage-sensitive dye imaging. *J Neurosci* 2001; **21**: 8435–8446.

504 5 Okubo Y, Sekiya H, Namiki S, Sakamoto H, Iinuma S, Yamasaki M *et al.* Imaging
505 extrasynaptic glutamate dynamics in the brain. *Proceedings of the National Academy of*
506 *Sciences* 2010; **107**: 6526–6531.

507 6 Crescenzi R, DeBrosse C, Nanga RPR, Byrne MD, Krishnamoorthy G, D'Aquilla K *et al.*
508 Longitudinal imaging reveals subhippocampal dynamics in glutamate levels associated with
509 histopathologic events in a mouse model of tauopathy and healthy mice. *Hippocampus* 2017;
510 **27**: 285–302.

511 7 Voets NL, Hodgetts CJ, Sen A, Adcock JE, Emir U. Hippocampal MRS and subfield volumetry
512 at 7T detects dysfunction not specific to seizure focus. *Sci Rep* 2017; **7**: 1–14.

513 8 Kondo M, Kobayashi K, Ohkura M, Nakai J, Matsuzaki M. Two-photon calcium imaging of the
514 medial prefrontal cortex and hippocampus without cortical invasion. *Elife* 2017; **6**: 592.

515 9 Wang LV, Hu S. Photoacoustic tomography: in vivo imaging from organelles to organs. *Science*
516 2012; **335**: 1458–1462.

517 10 Wang X, Pang Y, Ku G, Xie X, Stoica G, Wang LV. Noninvasive laser-induced photoacoustic
518 tomography for structural and functional in vivo imaging of the brain. *Nat Biotechnol* 2003; **21**:
519 803–806.

520 11 Zhang HF, Maslov K, Stoica G, Wang LV. Functional photoacoustic microscopy for high-
521 resolution and noninvasive in vivo imaging. *Nat Biotechnol* 2006; **24**: 848–851.

522 12 Kang J, Kim E-K, Kim GR, Yoon C, Song T-K, Chang JH. Photoacoustic imaging of breast
523 microcalcifications: a validation study with 3-dimensional ex vivo data and spectrophotometric
524 measurement. *J Biophoton* 2015; **8**: 71–80.

525 13 Kang J, Chung WY, Kang S-W, Kwon HJ, Yoo J, Kim E-K *et al.* Ex Vivo Estimation of
526 Photoacoustic Imaging for Detecting Thyroid Microcalcifications. *PLoS ONE* 2014; **9**.
527 doi:10.1371/journal.pone.0113358.

528 14 Kim GR, Kang J, Kwak JY, Chang JH, Kim SI, Youk JH *et al.* Photoacoustic imaging of breast
529 microcalcifications: a preliminary study with 8-gauge core-biopsied breast specimens. *PLoS*
530 *ONE* 2014; **9**: e105878.

531 15 Yao J, Maslov KI, Wang LV. In vivo Photoacoustic Tomography of Total Blood Flow and
532 Potential Imaging of Cancer Angiogenesis and Hypermetabolism. *Technol Cancer Res Treat*
533 2012; **11**: 301–307.

534 16 Hu S. Listening to the Brain With Photoacoustics. *IEEE J Select Topics Quantum Electron*
535 2016; **22**: 117–126.

536 17 Hui J, Cao Y, Zhang Y, Kole A, Wang P, Yu G *et al.* Real-time intravascular photoacoustic-
537 ultrasound imaging of lipid-laden plaque in human coronary artery at 16 frames per second. *Sci*
538 *Rep* 2017; **7**: 1417.

539 18 Wu M, Springeling G, Lovrak M, Mastik F, Iskander-Rizk S, Wang T *et al.* Real-time
540 volumetric lipid imaging in vivo by intravascular photoacoustics at 20 frames per second.
541 *Biomed Opt Express* 2017; **8**: 943–953.

542 19 Kang J, Zhang HK, Kadam SD, Fedorko J, Valentine H, Malla AP *et al.* Transcranial Recording
543 of Electrophysiological Neural Activity in the Rodent Brain in vivo Using Functional
544 Photoacoustic Imaging of Near-Infrared Voltage-Sensitive Dye. *Frontiers in Neuroscience*
545 2019; **13**: 1–14.

546 20 Andrade-Valenca LP, Dubeau F, Mari F, Neurology RZ, 2011. Interictal scalp fast oscillations
547 as a marker of the seizure onset zone. *Neurology* 2011; **77**: 524–531.

548 21 Foldvary N, Klem G, Hammel J, Bingaman W, Najm I, Lüders H. The localizing value of ictal
549 EEG in focal epilepsy. *Neurology* 2001; **57**: 2022–2028.

550 22 Paxinos G, Watson C. *The Rat Brain in Stereotaxic Coordinates*. Seventh edition. Elsevier
551 Academic Press, 2014.

552 23 Pak RW, Kang J, Valentine H, Loew LM, Thorek DL, Boctor EM *et al.* Voltage-sensitive dye
553 delivery through the blood brain barrier using adenosine receptor agonist Regadenoson. *Biomed*
554 *Opt Express* 2018; **9**: 3915–3922.

555 24 Nie L, Cai X, Maslov K, Garcia-Uribe A, Anastasio MA, Wang LV. Photoacoustic tomography
556 through a whole adult human skull with a photon recycler. *J Biomed Opt* 2012; **17**: 110506.

557 25 Li W, Chen R, Lv J, Wang H, Liu Y, Peng Y *et al.* In Vivo Photoacoustic Imaging of Brain
558 Injury and Rehabilitation by High-Efficient Near-Infrared Dye Labeled Mesenchymal Stem
559 Cells with Enhanced Brain Barrier Permeability. *Adv Sci (Weinh)* 2018; **5**: 1700277–11.

560 26 Liu Y, Yang Y, Sun M, Cui M, Fu Y, Lin Y *et al.* Highly specific noninvasive photoacoustic
561 and positron emission tomography of brain plaque with functionalized croconium dye labeled
562 by a radiotracer. *Chem Sci* 2017; **8**: 2710–2716.

563 27 Hu S, Wang LV. Neurovascular photoacoustic tomography. *Front Neuroenergetics* 2010; **2**: 10.

564 28 Zhang P, Li L, Lin L, Hu P, Shi J, He Y *et al.* High-resolution deep functional imaging of the
565 whole mouse brain by photoacoustic computed tomography in vivo. *J Biophoton* 2018; **11**:
566 e201700024–6.

567 29 Luke GP, Yeager D, Emelianov SY. Biomedical Applications of Photoacoustic Imaging with
568 Exogenous Contrast Agents. *Ann Biomed Eng* 2011; **40**: 422–437.

569 30 Weber J, Beard PC, Bohndiek SE. Contrast agents for molecular photoacoustic imaging. *Nat*
570 *Meth* 2016; **13**: 639–650.

571 31 Huynh E, Jin CS, Wilson BC, Zheng G. Aggregate enhanced trimodal porphyrin shell
572 microbubbles for ultrasound, photoacoustic, and fluorescence imaging. *Bioconjugate Chem*
573 2014; **25**: 796–801.

574 32 Ju K-Y, Kang J, Pyo J, Lim J, Chang JH, Lee J-K. pH-Induced aggregated melanin
575 nanoparticles for photoacoustic signal amplification. *Nanoscale* 2016; **8**: 14448–14456.

576 33 Moon H, Kang J, Sim C, Kim J, Lee H, Chang JH *et al.* Multifunctional theranostic contrast
577 agent for photoacoustics- and ultrasound-based tumor diagnosis and ultrasound-stimulated local
578 tumor therapy. *Journal of Controlled Release* 2015; **218**: 63–71.

579 34 Deán-Ben XL, Sela G, Lauri A, Kneipp M, Ntziachristos V, Westmeyer GG *et al.* Functional
580 optoacoustic neuro-tomography for scalable whole-brain monitoring of calcium indicators. *Light*
581 *Sci Appl* 2016; **5**: e16201–7.

582 35 Roberts S, Seeger M, Jiang Y, Mishra A, Sigmund F, Stelzl A *et al.* Calcium Sensor for
583 Photoacoustic Imaging. *J Am Chem Soc* 2018; **140**: 2718–2721.

584 36 Ruo B, Zhang R, Li L, Shao J-Y, Wang LV. Photoacoustic imaging of voltage responses beyond
585 the optical diffusion limit. *Sci Rep* 2017; **7**: 2560.

586 37 Nowak K, Mix E, Gimsa J, Strauss U, Sriperumbudur KK, Benecke R *et al.* Optimizing a
587 Rodent Model of Parkinson's Disease for Exploring the Effects and Mechanisms of Deep Brain
588 Stimulation. *Parkinson's Disease* 2011; **2011**: 1–19.

589 38 Zhang HK, Yan P, Kang J, Abou DS, Le HND, Jha AK *et al.* Listening to membrane potential:
590 photoacoustic voltage-sensitive dye recording. *J Biomed Opt* 2017; **22**: 045006.

591 39 Szabo GG, Du X, Oijala M, Varga C, Parent JM, Soltesz I. Extended Interneuronal Network of
592 the Dentate Gyrus. *Cell Rep* 2017; **20**: 1262–1268.

593 40 Johnston MV, Ammanuel S, O'Driscoll C, Wozniak A, Naidu S, Kadam SD. Twenty-four hour
594 quantitative-EEG and in-vivo glutamate biosensor detects activity and circadian rhythm
595 dependent biomarkers of pathogenesis in Mecp2 null mice. *Front Syst Neurosci* 2014; **8**: 118.

596 41 Medina-Ceja L, Pardo-Peña K, Morales-Villagrán A, Ortega-Ibarra J, López-Pérez S. Increase
597 in the extracellular glutamate level during seizures and electrical stimulation determined using a
598 high temporal resolution technique. *BMC Neurosci* 2015; **16**: 11.

599 42 Clay M, Monbouquette HG. A Detailed Model of Electroenzymatic Glutamate Biosensors To
600 Aid in Sensor Optimization and in Applications in Vivo. *ACS Chem Neurosci* 2018; **9**: 241–251.

601 43 Moon J-M, Thapliyal N, Hussain KK, Goyal RN, Shim Y-B. Conducting polymer-based
602 electrochemical biosensors for neurotransmitters: A review. *Biosens Bioelectron* 2018; **102**:
603 540–552.

604 44 Sauleau P, Lapouble E, Val-Laillet D, Malbert CH. The pig model in brain imaging and
605 neurosurgery. *Animal* 2009; **3**: 1138–1151.

606 45 Kang J, Boctor EM, Adams S, Kulikowicz E, Zhang HK, Koehler RC *et al.* Validation of
607 noninvasive photoacoustic measurements of sagittal sinus oxyhemoglobin saturation in hypoxic
608 neonatal piglets. *J Appl Physiol* 2018; **125**: 983–989.

609 46 American National Standard for the Safe Use of Lasers. *Annals of Internal Medicine* 1975; **82**:
610 132.

611 47 Baumann MH, Ayestas MA, Partilla JS, Sink JR, Shulgin AT, Daley PF *et al.* The designer
612 methcathinone analogs, mephedrone and methylone, are substrates for monoamine transporters
613 in brain tissue. *Neuropsychopharmacology* 2012; **37**: 1192–1203.

614 48 Elmore JS, Dillon-Carter O, Partilla JS, Ellefsen KN, Concheiro M, Suzuki M *et al.*
615 Pharmacokinetic Profiles and Pharmacodynamic Effects for Methylone and Its Metabolites in
616 Rats. *Neuropsychopharmacology* 2017; **42**: 649–660.

617 49 Airan RD, Meyer RA, Ellens NPK, Rhodes KR, Farahani K, Pomper MG *et al.* Noninvasive
618 Targeted Transcranial Neuromodulation via Focused Ultrasound Gated Drug Release from
619 Nanoemulsions. *Nano Lett* 2017; **17**: 652–659.

620 50 Kang SK, Ammanuel S, Thodupunuri S, Adler DA, Johnston MV, Kadam SD. Sleep
621 dysfunction following neonatal ischemic seizures are differential by neonatal age of insult as
622 determined by qEEG in a mouse model. *Neurobiol Dis* 2018; **116**: 1–12.

623

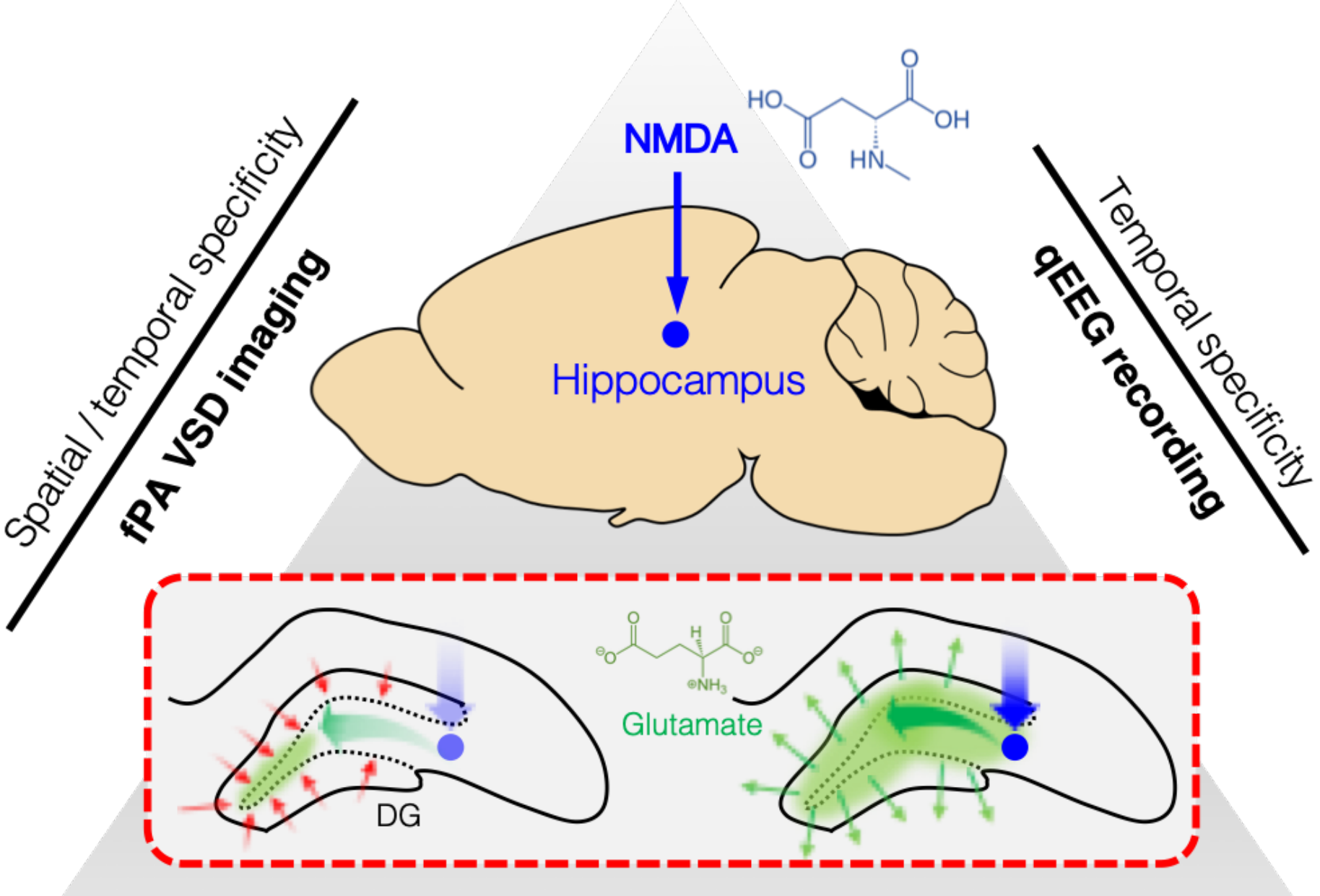

Microdialysis

Focal neurochemical specificity

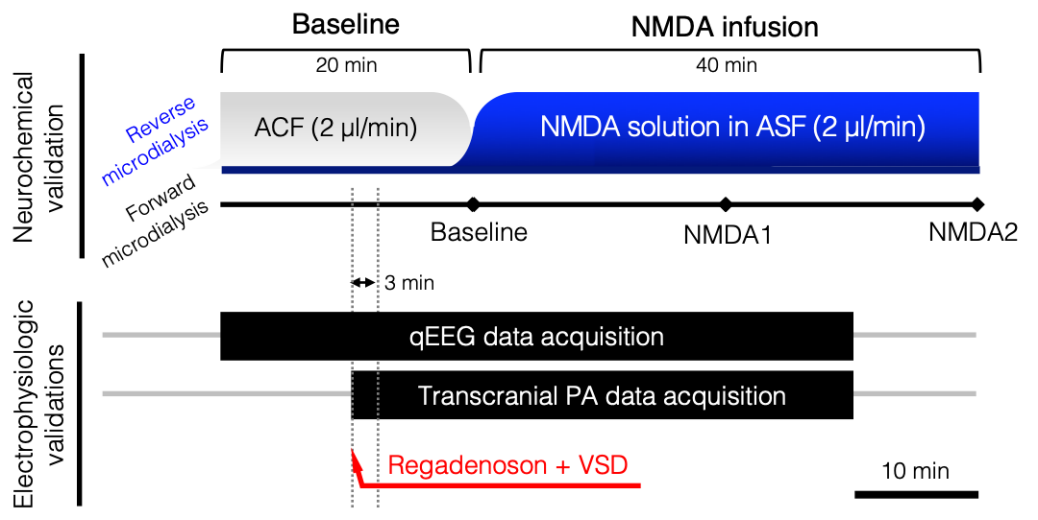
Baseline
NMDA infusion
20 min
40 min
Neurochemical validation
Reverse microdialysis
ACF (2 µl/min)
NMDA solution in ASF (2 µl/min)
Forward microdialysis
Baseline
NMDA1
NMDA2
3 min
Electrophysiologic validations
qEEG data acquisition
Transcranial PA data acquisition
Regadenoson + VSD
10 min

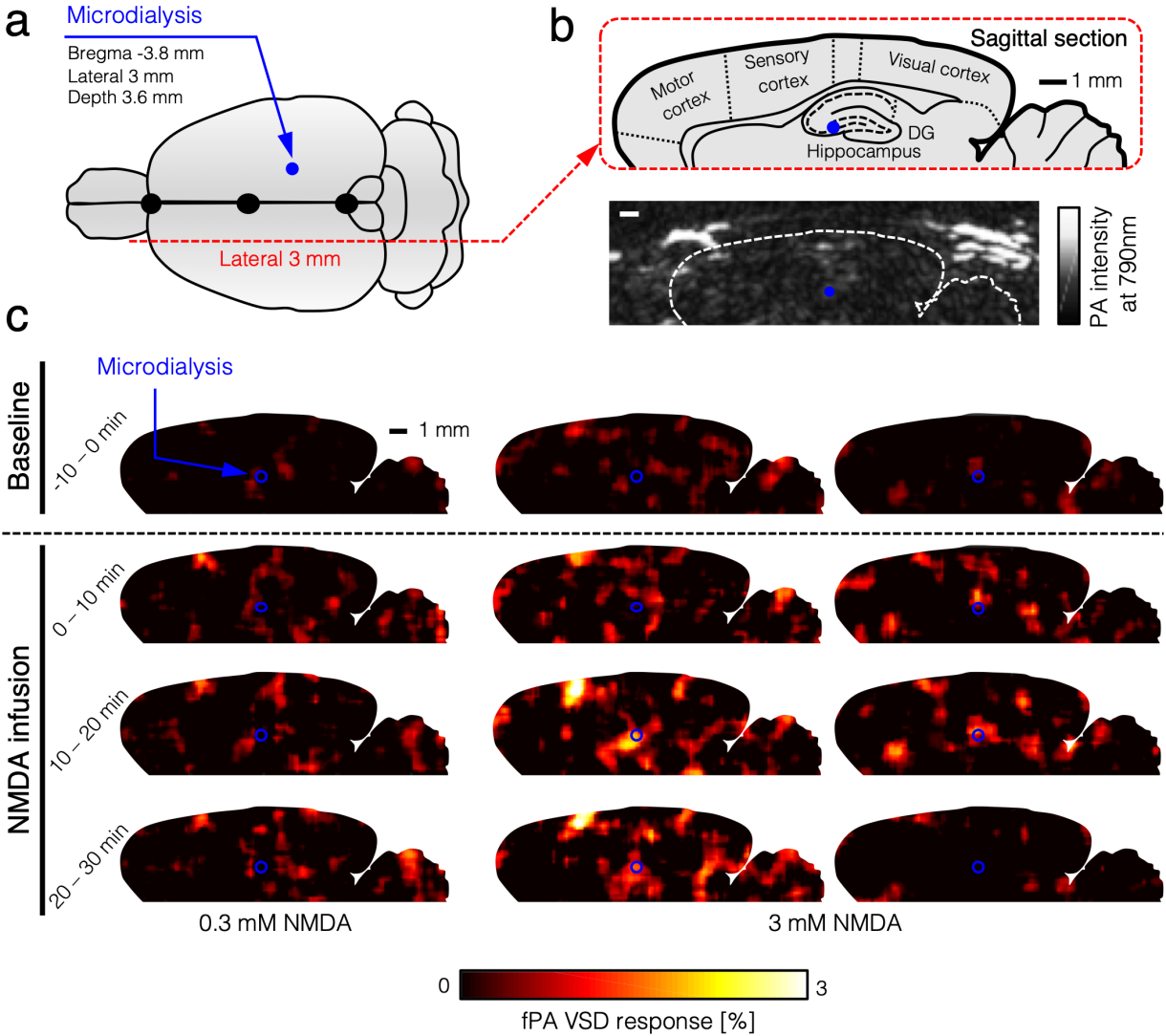
a
Microdialysis
Bregma -3.8 mm
Lateral 3 mm
Depth 3.6 mm
Lateral 3 mm
b
Sagittal section
Motor cortex
Sensory cortex
Visual cortex
1 mm
DG
Hippocampus
PA intensity at 790nm
c
Baseline
Microdialysis
-10 – 0 min
1 mm
NMDA infusion
0 – 10 min
10 – 20 min
20 – 30 min
0.3 mM NMDA
3 mM NMDA
0
3
fPA VSD response [%]

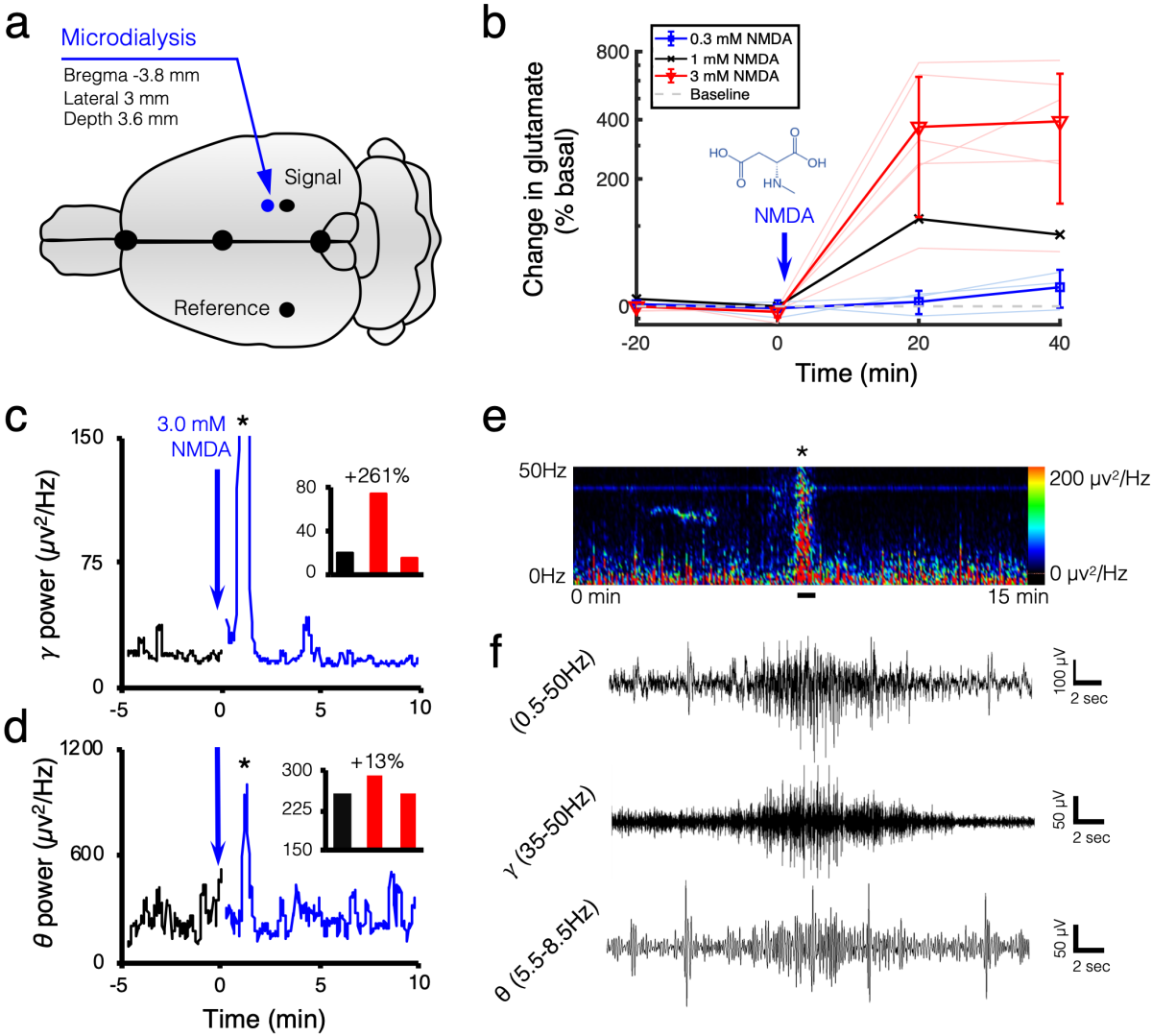
a
Microdialysis
Bregma -3.8 mm
Lateral 3 mm
Depth 3.6 mm
Signal
Reference
b
0.3 mM NMDA
1 mM NMDA
3 mM NMDA
Baseline
Change in glutamate (% basal)
800
400
200
0
-20
0
20
40
Time (min)
NMDA
c
3.0 mM NMDA
*
+261%
γ power (μv²/Hz)
150
75
0
-5
0
5
10
d
*
+13%
θ power (μv²/Hz)
1200
600
0
Time (min)
e
*
50Hz
0Hz
200 μv²/Hz
0 μv²/Hz
0 min
15 min
f
(0.5-50Hz)
γ (35-50Hz)
θ (5.5-8.5Hz)
100 μV
50 μV
2 sec

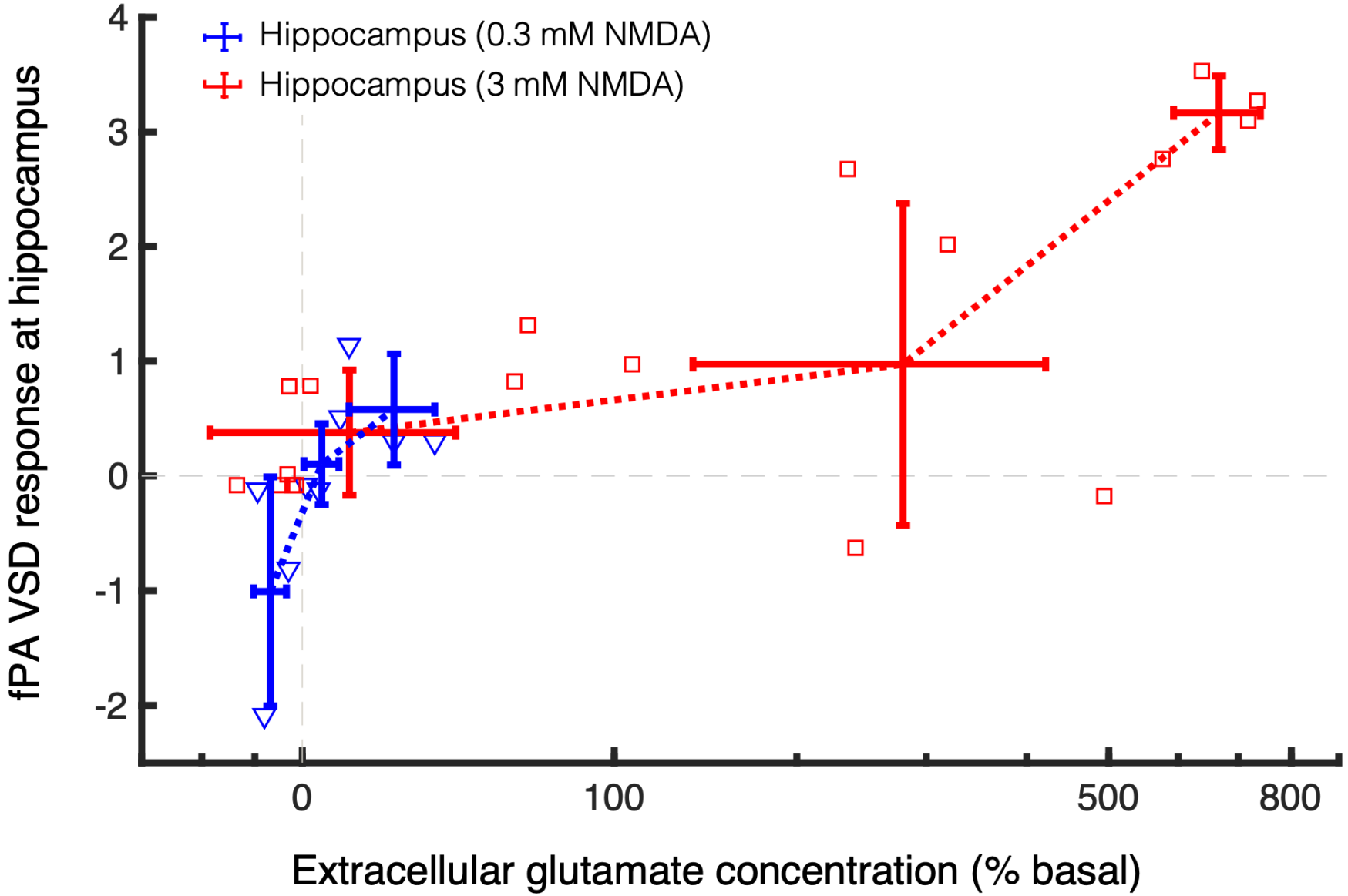
Hippocampus (0.3 mM NMDA)
Hippocampus (3 mM NMDA)
fPA VSD response at hippocampus
4
3
2
1
0
-1
-2
0
100
500
800
Extracellular glutamate concentration (% basal)

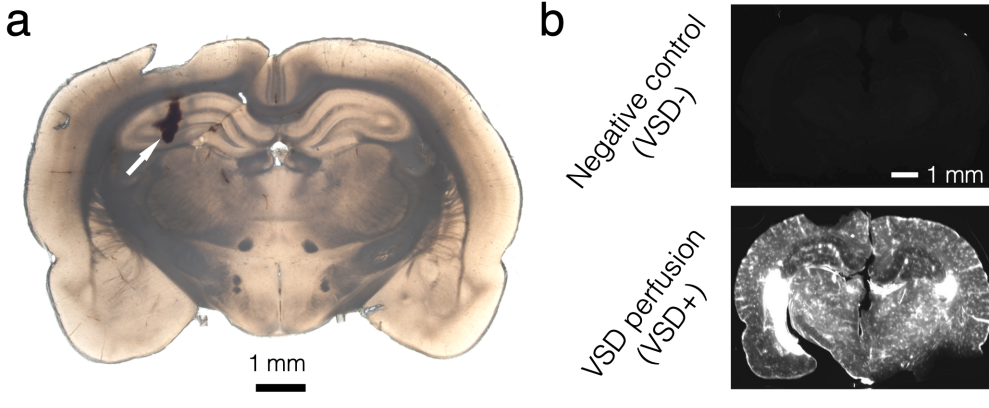
a
1 mm
b
Negative control
(VSD-)
1 mm
VSD perfusion
(VSD+)

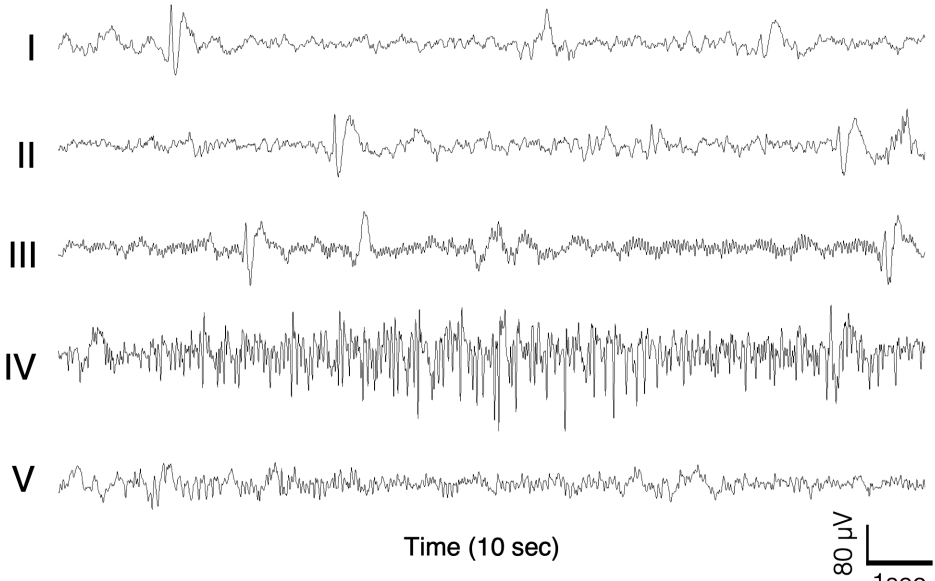
I
II
III
IV
V
Time (10 sec)
80 μV
1sec

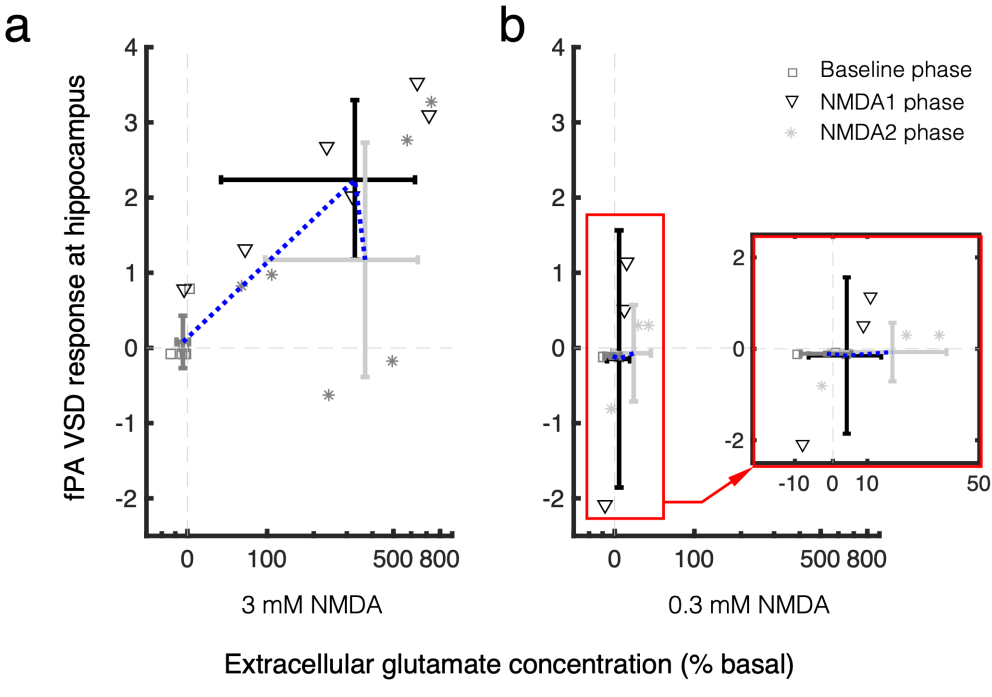
a
b
fPA VSD response at hippocampus
Baseline phase
NMDA1 phase
NMDA2 phase
4
3
2
1
0
-1
-2
0
100
500 800
3 mM NMDA
0.3 mM NMDA
-10
0
10
50
Extracellular glutamate concentration (% basal)